Feature Article

Visualization of Clouds and Atmospheric Air Flows

Noël Rimensberger, Markus Gross, and Tobias Günther
ETH Zürich

***Abstract*—The IEEE Scientific Visualization Contest 2017 addressed the arising challenges in the visualization and analysis of atmospheric cloud-resolving simulations. In this paper, we utilize direct and indirect methods to represent atmospheric attributes such as cloud water content and air pressure, and employ Eulerian and Lagrangian techniques for air flow visualization.**

The IEEE Scientific Visualization Contest 2017 concentrated on the cloud development and evolution over Germany. The data was provided by the German Climate Computing Center (DKRZ) and was simulated in the context of the HD(CP)^2 project.[1] The goal of this project was the simulation of high-resolution cloud data at an unprecedented level of detail, which sheds light onto the creation and evolution of highly complex dynamical cloud systems. For the contest, a subset of the simulation data was provided and participants were encouraged to apply state-of-the-art visualization techniques to support the three-dimensional (3-D) analysis of this multivariate spatiotemporal data set. For a comprehensive overview of common visualization methods for meteorological data, we refer to the recent survey of Rautenhaus *et al.*[2]

One of the current and future challenges of meteorological data analysis is the ever-growing size of the simulation data. A common visualization principle that is applicable in this case is the overview and detail paradigm, which provides an overview visualization that serves as an entry point for a more detailed analysis. Aside from the overviews that cover entire Germany, we focus our analysis on two regions of interests, which exhibit interesting weather situations. The first region is around Regensburg in Bavaria, which we call in the following the updraft region. The second region is around Paderborn, which is near Teutoburg Forest (Teutoburger Wald) and the Egge Hills (Eggegebirge), which we later refer to as the hill region.

Digital Object Identifier 10.1109/MCG.2018.2880821
Date of current version 6 March 2019.

Meteorological situation

We concentrate our analysis on two selected regions of interest around Regensburg and Paderborn. First, we describe the observed/measured weather conditions for the simulated day. April 26th 2013 was the warmest day in Regensburg in all April, but it was also a turning point.[3] From 25th to 27th, the air pressure dropped by 23 hPa, which marked the arrival of a low-

The 2017 IEEE Scientific Visualization Contest

Thomas Wischgoll – Wright State University
Niklas Röber – German Climate Computing Center
Amit Chourasia – San Diego Supercomputer Center, UCSD

Introduction

Each year, the IEEE Scientific Visualization Contest presents researchers from the visualization community an opportunity to transfer the latest developments in visual data analysis to a challenging, real-world application scenario. Details on this year's event and past contests are available via http://sciviscontest.ieeevis.org.

The Contest Problem

For 2017, the contest was dedicated to the visualization and analysis of large and complex atmospheric simulations. The data originates from the HD(CP)^2 project and shows the weather situation above Germany for April 26, 2013. The output generated by climate simulations is increasing in size, as well as complexity. Both aspects pose equal challenges for the visualization and interactive analysis of the data. The increase in complexity is due to maturing models that are able to better describe the intricacies of the climate system, while the gain in data size is a direct result of an increased spatial and temporal resolution used by modern climate models. The benefit of these high resolution models is not only that they are able to simulate the Earth's past, current and future climate with a higher accuracy, these models also allow us to gain more insight in the complexity of the weather and climate system itself. Until very recently, clouds and precipitation processes were only approximated within climate models and not fully resolved. Now, with maturing models and increasing computational capacities, we are not only able to really simulate clouds and precipitation processes in global models, but also small scale features from the formation of clouds, ice and rain. The data generated, however, is huge and requires special methods for the analysis and visualization of very large data sets.

Evaluation

We received four submissions for the 2017 SciVis contest. A jury of five domain scientists and visualization researchers (Matthias Brück, Ksenia Gorges, Rieke Heinze, John Clyne, Alexander Kuhn, Theresa-Marie Rhyne, and Niklas Röber) carefully reviewed all entries. Since the main goal of the visualization contests is to demonstrate applicability of cutting-edge visualization research to a specific domain, the review team was assembled with the emphasis on the application domain. This underscores the importance for a successful entry to provide insightful visualizations that help the domain scientists in their analysis of the data.

The jury selected the entry "Visualization of Clouds and Atmospheric Air Flows" by Noël Rimensberger, Markus Gross, and Tobias Günther all of whom are with the Computer Graphics Laboratory at ETH Zürich as the overall contest winner. The presented paper is an extended discussion of their results. However, this year's decision was extremely close that the jury decided to award an "Honorable Mention" to the entry "STRIELAD - A Scalable Toolkit for Real-time Interactive Exploration of Large Atmospheric Datasets" by Simon Schneegans, Lori Neary, Markus Flatken, and Andreas Gerndt from the Department of Simulation and Software Technology at the German Aeropsace Center and the Institut royal d'Aronomie Spatiale de Belgique.

Acknowledgments

The data set for this contest has been kindly provided by the German Climate Computing Center as part of the HD(CP)^2 Project. We would like to especially thank the contest jury for their continued support throughout the entire contest.

pressure area. From 26th to 28th, the maximum day temperature decreased from 27 °C to 12 °C. On April 26th, we observe strong updraft and cloud development in the simulation, which might be caused by the high surface temperature. The second region is around Paderborn, which is near Teutoburg Forest (Teutoburger Wald) and the Egge Hills (Eggegebirge), which we later refer to as the hill region.[4] From April 25th to 26th, the temperature decreased from 20 °C to 7 °C, while the air pressure dropped by 12 hPa. The updrafts and cloud dynamics in this region are influenced by the topography, as we will show later.

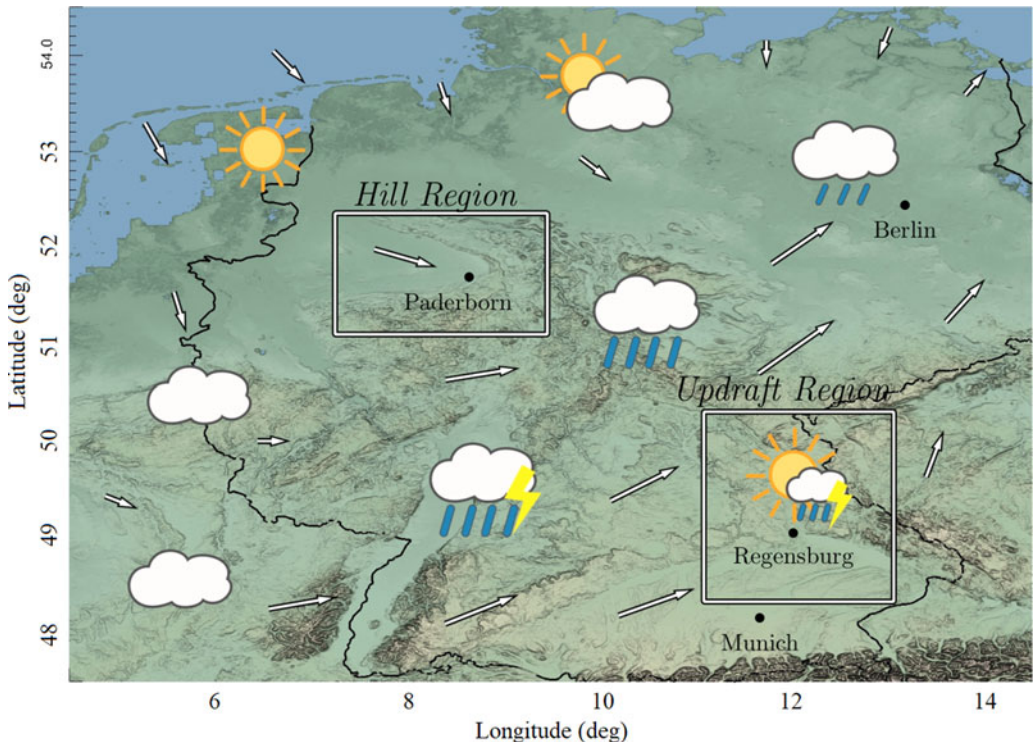

Figure 1. This figure shows an overview of the observed/measured weather conditions in the evening (19:00) of April 26, 2013. The glyphs provide an approximate depiction based on actual weather reports at that time. We highlighted the two regions of interest (hill region and updraft region), which we discuss in more detail in the remainder of the paper. As shown later, the contest simulation data resembles these weather reports closely.

Data preprocessing

The numerical simulations were computed on icosahedral grids, which are referred to as ICON grids. For ease of data handling, a resampled version onto rectilinear grids was also provided with the contest data. Most of our visualizations are based on the four-hour time series of the resampled data set. To ease the data handling and to facilitate the work with consumer hardware, we split the data into smaller chunks. We prepared a single VTK ImageData (.vti) file for each attribute and per time step. The complete region was down-sampled and selected regions of interest were extracted from the provided rectilinear grid to show the regions of interest at highest resolution. The longitude/latitude/height ranges and the grid resolution of the regions are:

- Complete region: [4.50°–14.5°]/[47.5°–54.5°]/[0.11–20.8 km], 286 × 311 × 150;
- Updraft region: [11.1°–13.4°]/[48.3°–50.1°]/[0.11–20.8 km], 315 × 401 × 150;
- Hill region: [7.00°–9.20°]/[50.9°–52.5°]/[0.11–5.87 km], 316 × 357 × 70.

The file sizes range between 356–506 kB in 2-D and 32–76 MB in 3-D per time step per scalar attribute. For each region of interest and for each attribute a total of 240 files with a temporal resolution of 1 min was prepared.

The complete region covers the entirety of Germany. The updraft region is located around Regensburg and as mentioned above the smaller regions are resampled at higher resolution to provide more details. The hill region extends around the forested hills of the Teutoburg Forest (Teutoburger Wald) and the Egge Hills (Eggegebirge) in the state of North Rhine-Westphalia.

Figure 1 shows the extent of the selected regions on the map of Germany. Additionally, an overview of the observed/measured weather conditions is given, with a weather map that is based on the given contest data and historic weather reports.[3,4]

Published by the IEEE Computer Society IEEE Computer Graphics and Applications

Visualizations

The provided data shows the weather situation above Germany for April 26, 2013 from 17:00 to 21:00. The given spatial and temporal domain contains several interesting phenomena that we elaborate on in this section. First, rain bands and thick clouds across Germany dominate the picture, with one separated rain cloud in the south-east. In addition, turbulence can be observed at different locations and in varying altitudes. Following the research challenges posed by the contest, we look more closely into several of these interesting phenomena, and to this end, utilize multiple visualization techniques.

General visualizations

We begin with a number of general visualizations to familiarize with the given data.

Clouds, Rain, and Ice First, we look at the cloud and rain properties at 19:00 on the whole spatial domain of Germany, namely cloud water content (CLW), cloud ice content (CLI) and the rain mixing ratio (QR).

For an overview, Figure 2 shows various visualizations of the given meteorological attributes, helping in the investigation of the weather situation. In the top row, cloud water content (CLW) is visualized by volume rendering. The top view (left) resembles a realistic appearance as known from satellite images to make the map intuitive to read. Cloud cover and cloud thickness can be seen, while cloud height is only perceivable to some degree when viewing the tilted 3-D view (right).

In the second row of Figure 2, we visualize isosurfaces of the cloud water content and map air pressure values to color to improve the altitude visualization. The CLW-isovalue ($\mathrm{CLW} = 4 \times 10^{-4}\ \mathrm{kgkg}^{-1}$) cuts off cloud boundaries and minor clouds with low cloud water content. As a result, distinguishable and separated cloud structures appear instead of one big cloud body. As air pressure decreases almost linearly with increasing altitude, it is a helpful indicator of height that can complement a direct altitude visualization. Thus with this coloring, the height of the cloud top becomes visible in the top view, producing cloud layers that are distinguishable by air pressure. For instance, the color mapping allows us to easier distinguish low-lying fog (A) from vertically developed clouds (B). Additionally, vertical extents are visible in the tilted view.

The cloud water content ($\mathrm{CLW} = 4 \times 10^{-4}\,\mathrm{kgkg}^{-1}$), cloud ice content ($\mathrm{CLI} = 1.5 \times 10^{-4}\ \mathrm{kgkg}^{-1}$) and the rain mixing ratio ($\mathrm{QR} = 1 \times 10^{-4}\ \mathrm{kgkg}^{-1}$) are visualized in the third row of Figure 2 using isosurfaces. The tilted view provides an impression of the typical vertical stacking of the different hydrological fields, their spatial extent and coverage.

Since isosurfaces do not depict extrema, we choose different techniques to visualize the rain water. The bottom row of Figure 2 shows the total precipitable water vertically integrated per column and thus projected into 2-D on the left. The resulting precipitation map resembles known weather forecasts and radar images. Similar insights can be gained by the volume rendering of the rain mixing ratio (QR) values on the right. Again, the rain clouds that develop around Regensburg that are highlighted in the south-east of Germany are visible in both visualizations due to a strong precipitation in a small area.

Airplane trajectories We investigate the possible effects of the severe weather conditions on the flight paths in two ways. The visualization of flight paths in Figure 3 (top) allows us to directly look for deviations in the spatial domain. Here, all flight trajectories below 10 km are shown with the trajectories ranging from 19:00 to 19:12. Multiple flights take off eastwards from Frankfurt am Main straight through thick clouds with rainfall. One flight from Munich starts into the direction of the thick visible rain clouds. The arrow points to one flight from Munich slightly curving around the cumulonimbus cloud system at Regensburg. Though without data on original flight plans, we can only assume a deviation from the original path.

A more analytical approach is shown in Figure 3 (bottom). We study two of the bigger airports, Munich and Frankfurt, which are partially surrounded by severe weather conditions. The takeoff and landing directions (azimuth) throughout the day are plotted as points. This short-term data takes into account the first two available data points of the flight paths. The horizontal lines indicate the respective runways. From the preceding insights on the weather

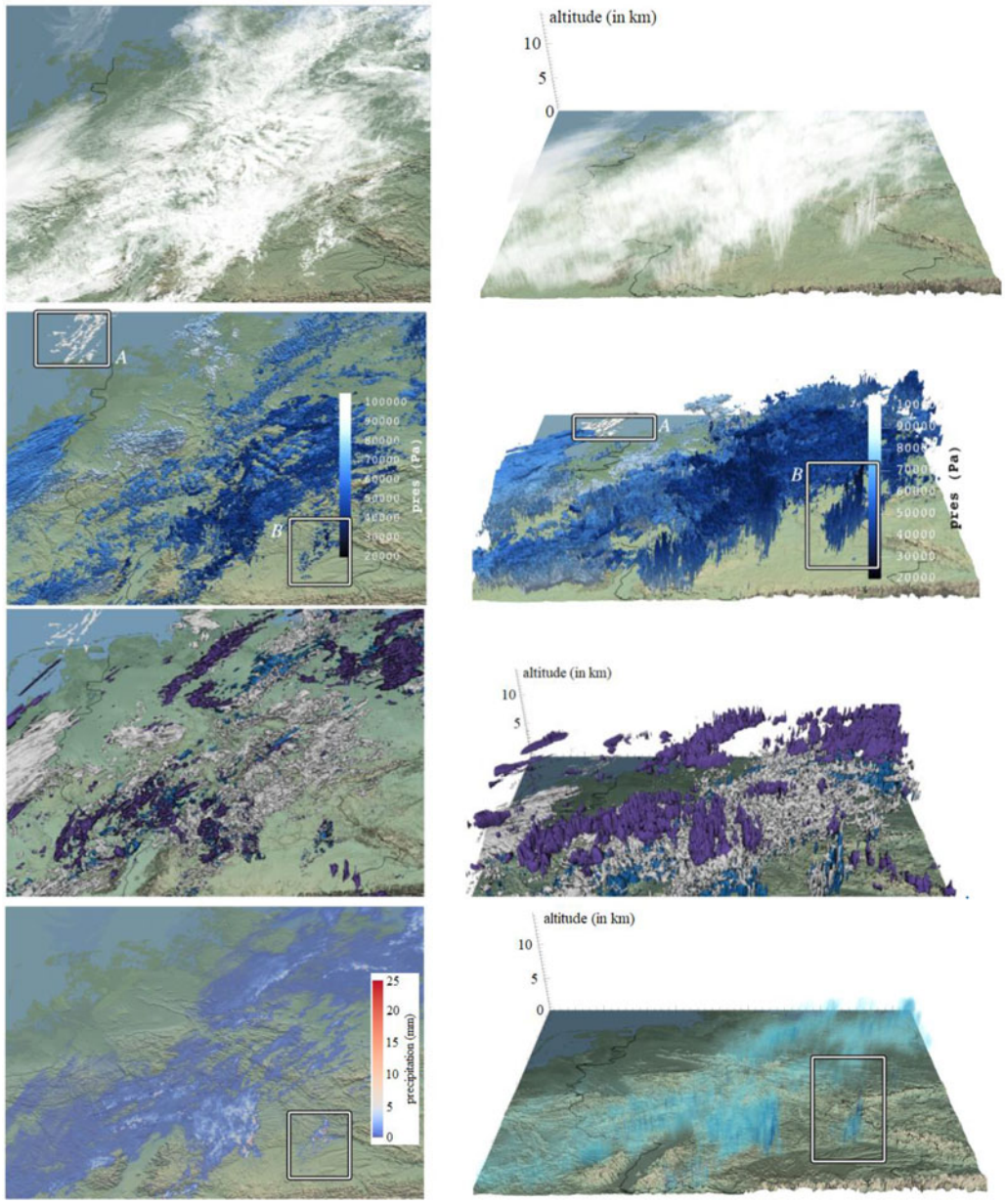

Figure 2. Basic visualizations of the provided meteorological attributes, including cloud water content, air pressure, cloud ice content, and the rain mixing ratio. In the 3-D visualizations, the vertical axis is scaled considerably to make the vertical structures more apparent.

situation, we could suspect runway changes around 19:00. But the figures show no clear evidence of any adjustments during the day. We conclude that the existing weather conditions were not severe enough for major adaptions.

Visualization of Wind

Vorticity and divergence To visualize a given time-dependent 3-D wind velocity field $\mathbf{v}(x, y, z, t)$, given by

$$\mathbf{v}(x, y, z, t) = (u(x, y, z, t), v(x, y, z, t), w(x, y, z, t))^T \quad (1)$$

a first approach is to study the wind by Eulerian visualizations of derived differential properties such as the vorticity magnitude $\|\nabla \times \mathbf{v}\|$ and the horizontal divergence $\nabla \cdot \mathbf{v} = \frac{\partial u}{\partial x} + \frac{\partial v}{\partial y}$. Figure 4 (top left) shows a direct volume rendering of the vorticity magnitude. Vorticity maxima appear near the ground due to boundary-induced shear,

Published by the IEEE Computer Society IEEE Computer Graphics and Applications

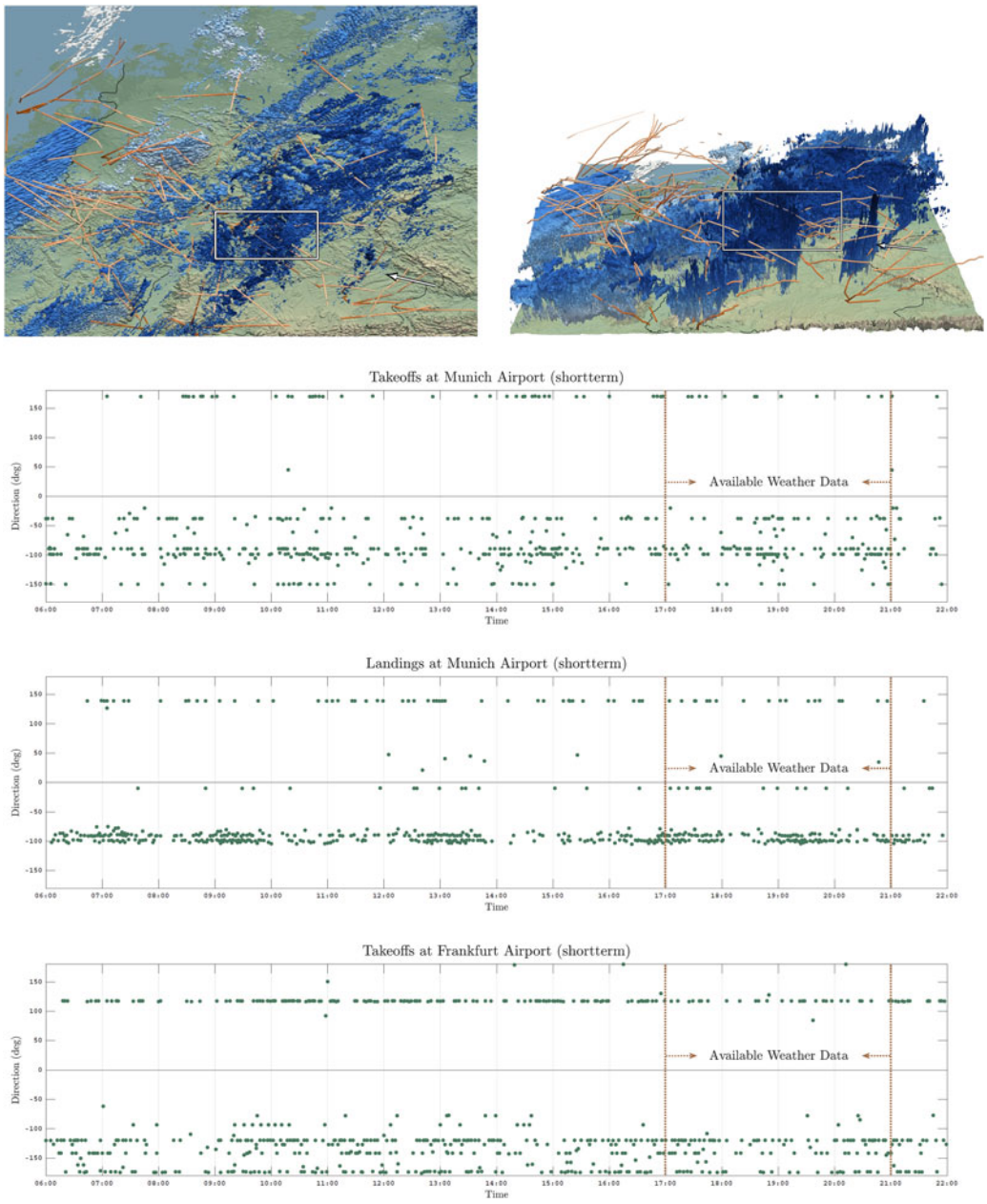

Figure 3. Analysis of air plane trajectories. The top figure plots the air plane trajectories on the map along with the air pressure isosurfaces similar to Figure 2. The three plots below show takeoff and landing directions for the airports in Munich and Frankfurt. Horizontal clusters are the runways, available at the airports. Despite the weather situation, no significant changes in the takeoff and landing directions are noticeable.

and at a higher altitude around 10 km. The high layers of vorticity can be an indication for the tropopause, which is the boundary layer between troposphere and stratosphere. Here, wind shear may lead to clear air turbulence and vortices.[5]

The volume rendering of horizontal divergence in Figure 4 (top right) looks more scattered. Two interesting spots in the south-east of Germany are highlighted. In both regions, we see clouds with high convergence near the ground and high divergence at higher levels. This is expected around vertically developed clouds with high updrafts.

In the bottom left of Figure 4, the relationship between clouds and vorticity is studied for the updraft region in south-east Germany. Here,

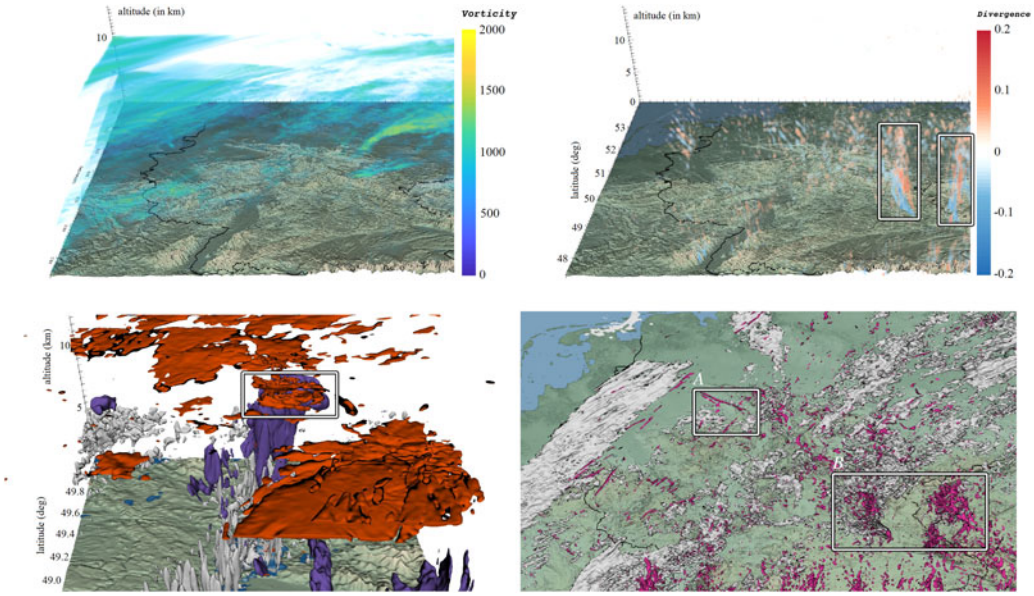

Figure 4. In the top row, volume renderings of vorticity (left) and horizontal divergence (right) are shown, indicating vorticity structures induced by shear and stacked divergence patterns due to updraft. In the left of the bottom row, the vorticity isosurface (red) on top of the cumulonimbus cloud is highlighted and on the right, isosurfaces of divergence and CLW reveal regions with divergence due to (A) orography and (B) divergence following the updraft. Both regions are highlighted.

vorticity isosurfaces (red) are shown in combination with a precipitation map on the ground, as well as CLW (white) and CLI (purple) isosurfaces that depict clouds. We see high values of vorticity developing at the top of the cumulonimbus cloud system. We will further discuss this phenomenon in the following paragraph on pathlines.

To differentiate between orography induced circulation and turbulence in clouds, we visualize the divergence using isosurfaces in the bottom right of Figure 4. There are two types of occurrences of high divergence. First, we see high divergence following the updrafts, and second, there are steady clusters around hill ranges, as highlighted in West Germany. One example of orography induced turbulence is discussed in more detail in the following paragraph.

Atmospheric trajectories We additionally provide a Lagrangian view on the wind data using pathlines. A pathline is the trajectory that a massless tracer particle follows in an unsteady vector field. In Figure 5 (top), we focus on the updraft and the turbulence around the cumulonimbus system in south-east Germany. We depict 4000 pathlines with an integration duration of 20 min, seeded at the cloud bottom. Most trajectories reach high altitudes due to updrafts, traveling from the cloud bottom to the top, where they flatten out and spread. The updraft is fairly turbulent with high vorticity values at different altitudes. To prevent occlusion only a small isosurface of the cloud water content (CLW $= 4 \times 10^{-4}$ kgkg^{-1}) is shown. The pathlines were computed with a fourth-order Runge-Kutta integrator. The step size was 5 s and the underlying flow field has a temporal resolution of 1 min.

To give an overview of all pathlines, we provide a focus and context visualization in Figure 5 (bottom). Using decoupled opacity optimization,[6] we fade out occluding pathlines that hinder the view on lines with the high updraft. This way, occlusion is avoided while further pathlines are shown as context.

An interesting phenomenon can be seen at the top of the cloud: Figure 6 shows a progression over time of pathlines colored by vorticity at the top of the cloud. As the rain clouds are passing by the seeding region, we can see high vorticity and turbulence from the coloring as well as from the lines themselves. Before and after the clouds arrive, two streaks

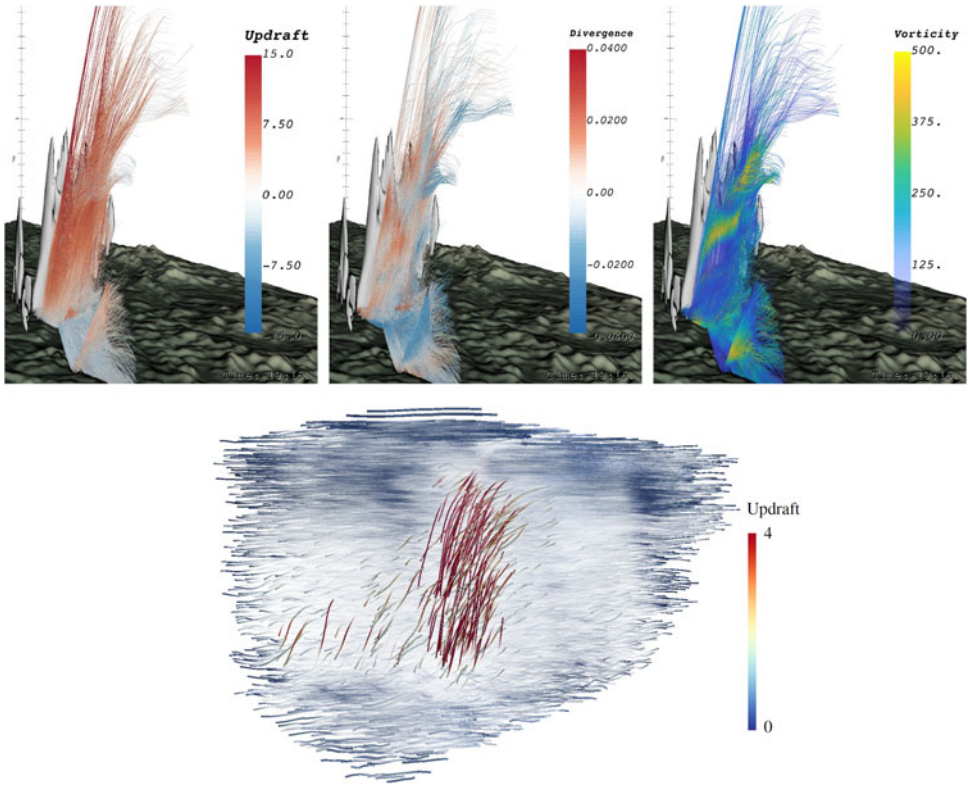

Figure 5. Visualizations of particle trajectories. The top row shows pathlines seeded at the cloud bottom of the cumulonimbus cloud in South-East Germany. At the bottom, a focus and context visualization of pathlines is shown in the same updraft region. Using decoupled opacity optimization, opacities are adjusted so that trajectories with high updraft are visible.

of high vorticity are noticeable, both arising from the wind shear at the height levels. Air masses moving with different speeds are visualized by the varying pathline lengths. The vorticity maxima are directly at the boundaries between those air masses, indicating shear-induced vorticity. Air masses moving with different speed can be an indication of the tropopause.

Figure 7 visualizes the orography-induced turbulence and compression at the windward side of the Teutoburg Forest and the Egge Hills. Winds coming from the west are forced upwards by the hills, and we can see an example of cloud formation due to orographic lift. The first three images show pathlines from 0 km to 3 km above the hill range with updraft, divergence, and vorticity color-coded on them, making an orography-induced updraft apparent. In the fourth image, isosurfaces of vorticity (orange) and divergence (pink) appear in the same location. Here, for the thresholds $\|\nabla \times \mathbf{v}\| = 250$ and $\nabla \cdot \mathbf{v} = -0.007$. The last row shows clouds with CLW isosurfaces ($\text{CLW} = 5 \times 10^{-4}\,\text{kgkg}^{-1}$), which line up along the hill range (bottom left) of the Teutoburg Forest and the Egge Hills. Pathlines indicate the forced updraft (bottom right).

Hyperbolic Lagrangian Coherent Structures

Finite-time Lyapunov exponents (FTLE) are a frequently used indicator for hyperbolic Lagrangian coherent structures, which act as transport barriers of tracer particles. The FTLE field is a Lagrangian measure that exhibits extremely thin ridge structures, which is why we used an unbiased Monte Carlo rendering approach[7] to visualize the transport barriers. Figure 8 shows the ground-induced turbulence, updraft columns and transport barriers at the tropopause for entire Germany and a selected region of interest around Regensburg. Ground turbulence is apparent particularly in the south (due to the Alps) and generally in the southern and eastern part of Germany. A comparison with Figure 2 depicts

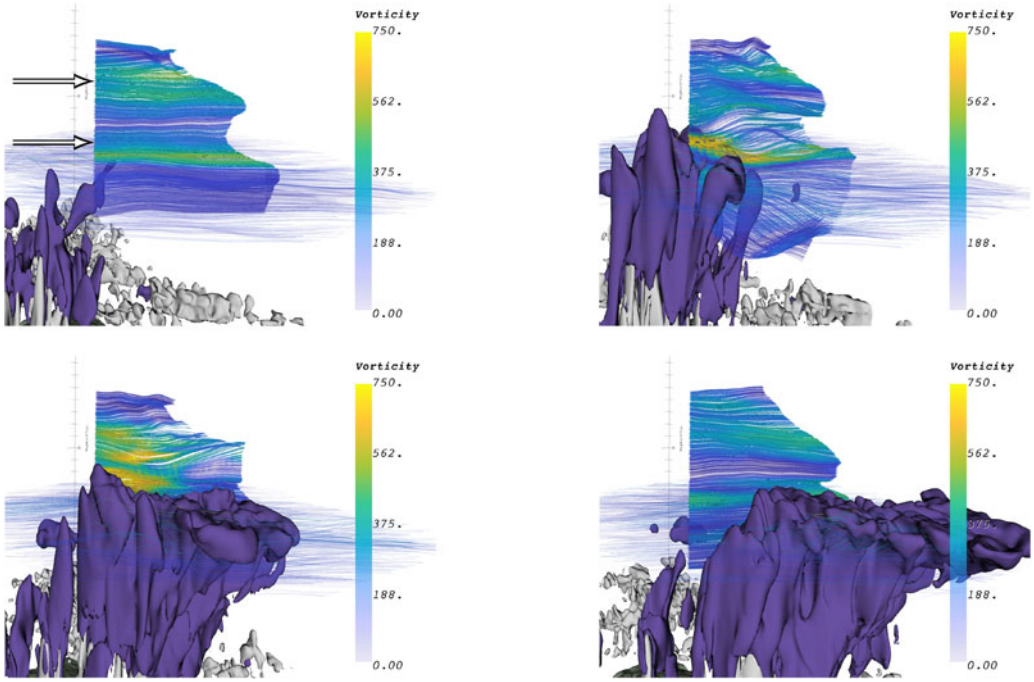

Figure 6. Visualization of the updraft region around Regensburg. Pathlines at the top of the cloud are colored by vorticity. The images show 15-min intervals as the cloud moves by. In the first time step (top left) streaks of high vorticity are highlighted, separating wind masses with different speeds. While the cloud passes by (top right and bottom left), updraft causes turbulence. Once the cloud has passed (bottom right), the air flow pattern returns back to its original state.

the reason: in the south, sunlight reaches the ground, causing a temperature-induced convection, paired with turbulence due to the arrival of a low-pressure area.

Comparing resolutions

The numerical simulations have been performed on three different grid resolutions. Deciding a-priori which grid resolutions to choose is very difficult, since the simulation time and the amount of required memory grow very quickly. Since simulation sizes are generally growing the question stands whether it is worth to put the additional effort of running a simulation at even higher resolution or whether a smaller grid resolution is sufficient. Using the 2-D ICON data with different resolutions, we computed difference maps, which are shown in Figure 9. We see considerable differences between the finest (Domain 3) and the coarsest (Domain 1) scale. The differences are particularly large for nonintegrated (local) attributes such as air pressure or cloud cover. Note that for those, the differences are larger at the cloud bottom than at the cloud top. A larger resolution is therefore useful for studies of the ground effect on the cloud development. We observed smaller differences for altitude-integrated attributes, such as CLWVI and CLIVI. Generally, we found that the most significant differences occurred at the boundaries of the clouds.

Cloud classification

Finally, after the detailed study of various visualizations, we present the results of two cloud classification schemes. The first scheme follows the World Meteorological Organization's International Cloud Atlas.[8] It mainly works with geometrical cloud height and altitude. Aside from low-level, mid-level and high-level clouds, two types of vertically developed clouds are distinguished: nimbostratus (Ns) and cumulonimbus (Cb). In addition to height information, precipitation is taken as indicator for Ns or Cb clouds.

The second approach is based on the classification scheme by the International Satellite Cloud Climatology Project (ISCCP)[9] and

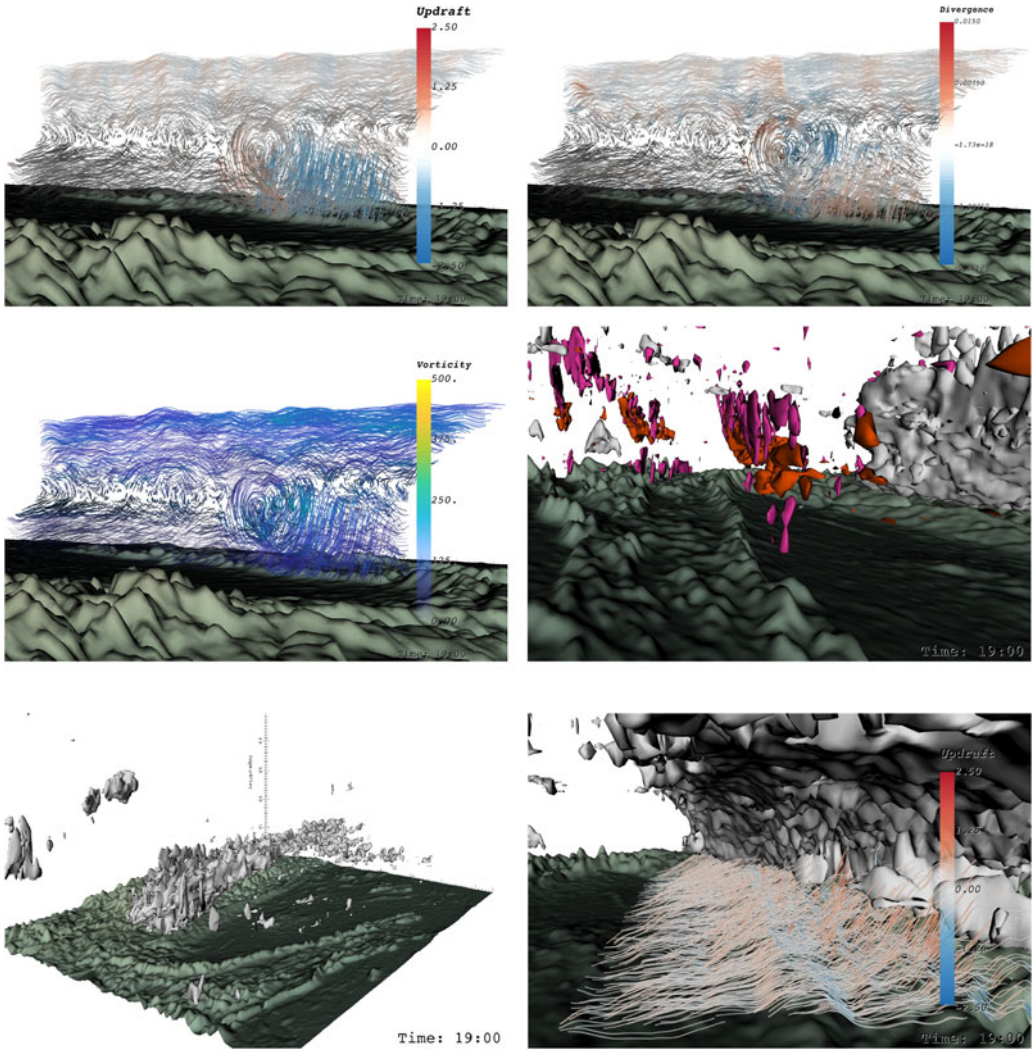

Figure 7. First three images show pathlines above the hill range with updraft, divergence, and vorticity, making an orography-induced updraft apparent. In the fourth image, isosurfaces of vorticity (orange) and divergence (pink) appear in the same location. Clouds, shown in the bottom row, line up along the hill range (left) of the Teutoburg Forest and the Egge Hills.

distinguishes nine cloud types. The scheme used by the ISCCP works for satellite imagery and depends on cloud optical thickness τ, which is a measure of the attenuation of light passing through a cloud. Stephens[10] shows that the cloud optical thickness is closely related to the liquid water path (LWP) of a cloud. The LWP is the amount of liquid water between two points, in this particular case between cloud bottom z_0 and cloud top z_1. It is defined as

$$\mathrm{LWP} = \int_{z_0}^{z_1} \rho_{\mathrm{air}} \cdot \mathrm{CLW}\, dz \qquad (2)$$

where ρ_{air} is the density of air. The density of *dry air* is

$$\rho_{\mathrm{air}} = \frac{p}{T \cdot R_{\mathrm{specific}}} \qquad (3)$$

where $R_{\mathrm{specific}} = 287.058\ \mathrm{J/(kg \cdot K)}$ is the specific gas constant of dry air, p is the air pressure (given as PRES) and T is the air temperature (given as TA). To obtain the density of *humid air*, we compute the virtual temperature T_v that a dry air mass would have in order to have the same density as humid air at temperature T, cf. Erneis:[11]

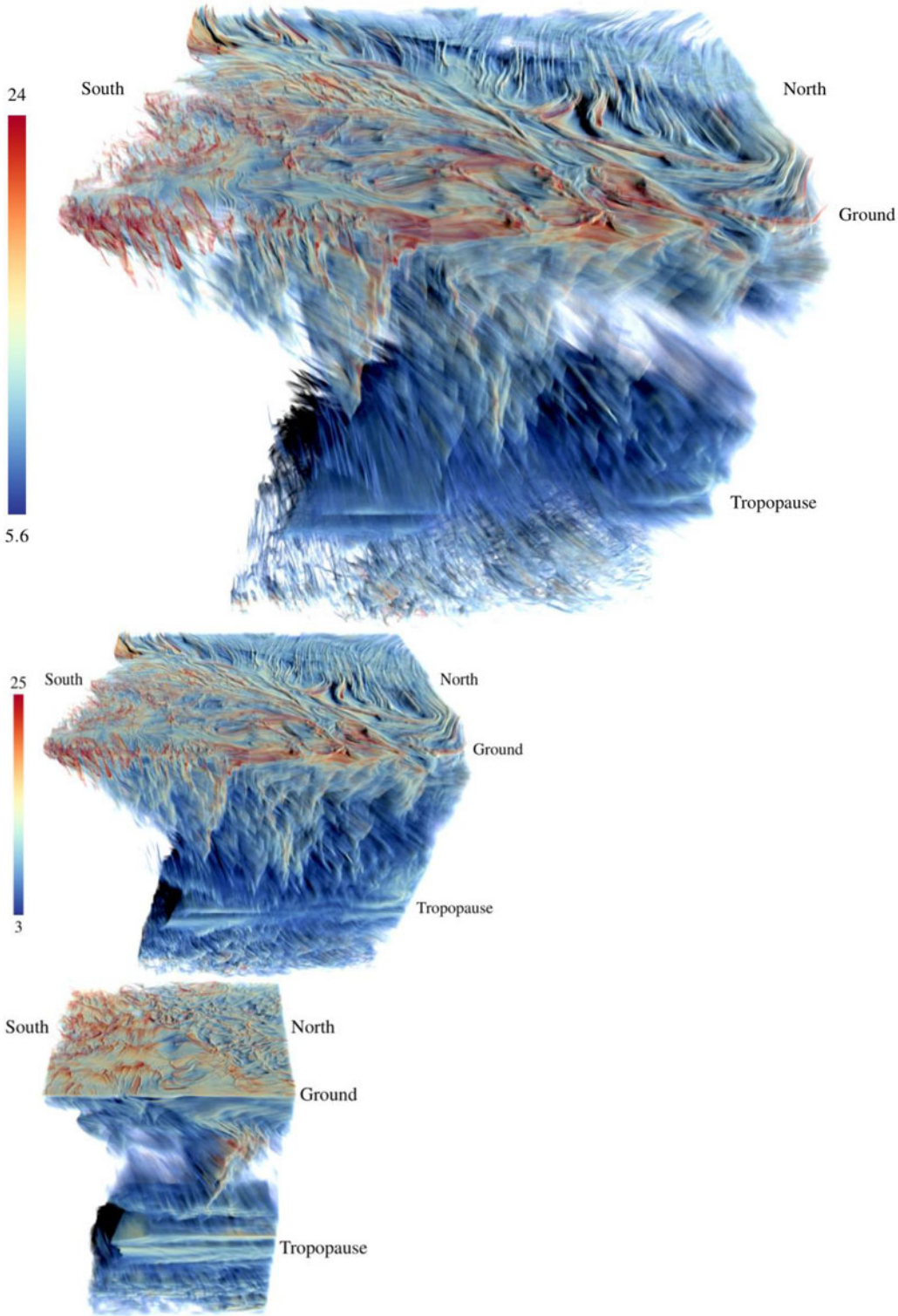

Figure 8. FTLE are an indicator for hyperbolic Lagrangian coherent structures, which act as transport barriers in vector fields. In these visualizations, altitude is reversed (ground is at the top) and North is right. All three images show the turbulent movement near the ground and updraft columns towards higher altitude. The FTLE layer at high altitudes (bottom) is the tropopause. Top and bottom left: entire Germany, Bottom right: updraft region around Regensburg. The two images of entire Germany differ by their transfer function.

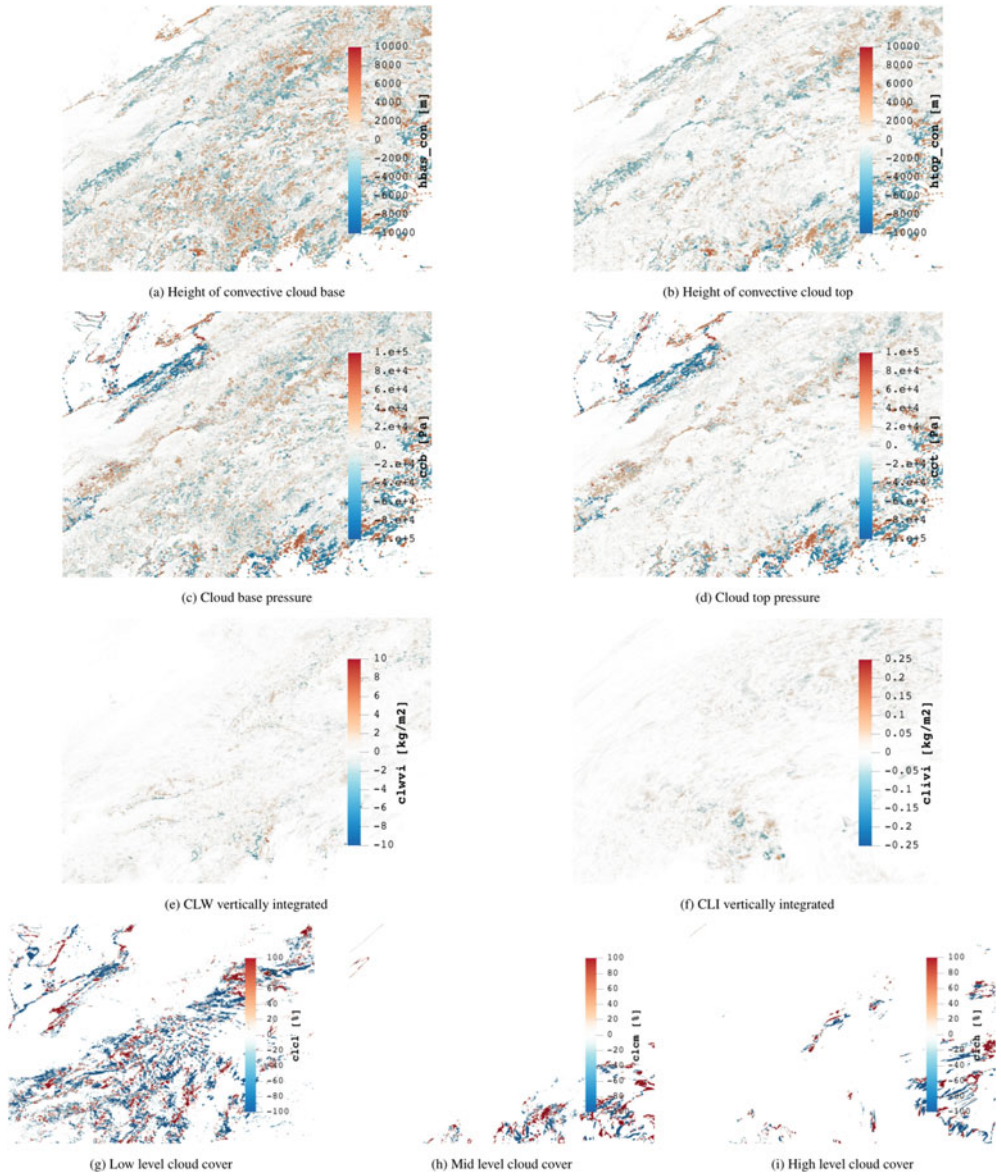

Figure 9. These visualizations display the differences between the finest (Domain 3) and the coarsest (Domain 1) ICON grid resolution. Areas in which the Domain 1 (low resolution) has higher values are indicated in blue. The other way around is indicated in red. Note that for height [(a) and (b)] and pressure [(c) and (d)] the difference maps are similar. For both, the differences at the cloud base [(a) and (c)] are bigger than at the cloud top [(b) and (d)]. The differences for vertically integrated measures are shown in (e) and (f), which are smaller. Finally, the cloud cover differences are shown for three different altitudes in (g), (h), and (i), indicating that the greatest differences occur at low altitudes.

$$T_v = T \cdot (1 + 0.609\ q) \tag{4}$$

where q is the specific humidity (given as in the contest data by the attribute HUS). The cloud optical thickness τ is then estimated using Stephens' relation:[10]

$$\log_{10}(\tau) \approx 0.2633 + 1.7095 \log_e(\log_{10}(\mathrm{LWP})). \tag{5}$$

Before clouds can be classified, they have to be detected. For this, we iterate over vertical columns in the atmosphere and look for vertically connected cloud components. A threshold on the cloud water content (CLW $= 1 \times 10^{-4}$ kgkg^{-1}) is used to determine whether a cloud is present or not. This way, multiple cloud layers can be distinguished within a single column. In contrast to

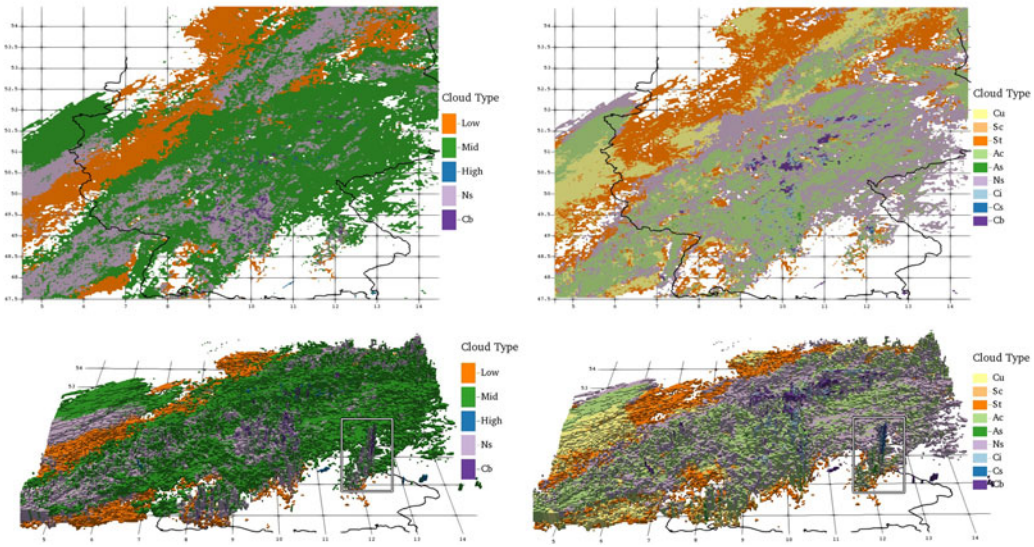

Figure 10. Here, the results of the two classification schemes are shown. In the left column, clouds are mainly distinguished by height level and additionally nimbostratus (Ns) and cumulonimbus (Cb) clouds are detected. The second approach on the right, which is based on the ISCCP classification scheme, distinguishes nine different cloud types. Low-level clouds are split into cumulus (Cu), stratocumulus (Sc), and stratus (St). Mid-level clouds are split into altocumulus (Ac) and altostratus (As). Finally, the high-level clouds are split into cirrus (Ci) and cirrostratus (Cs). Note that the two approaches agree in most parts, except that the second approach seems to have lower thresholds for nimbostratus and cumulonimbus clouds. The bottom row shows a 3-D visualization of the cloud classification. Both approaches classify the clouds around Regensburg as cumulonimbus cloud.

common classification approaches working on satellite imagery, we can thus detect clouds that otherwise would stay hidden. For each of those layers, we then determine the necessary properties such as geometrical cloud height, cloud top pressure or LWP that we later use for the actual classification. Each vertically connected cloud layer is classified by one of the approaches described above.

The resulting classifications are shown in Figure 10. Both visualizations show small fluctuations in the horizontal direction, due to the fact that horizontal connectivity is not considered. For the basic cloud levels, the two approaches agree in most parts, but a significant difference is seen in the classification of the cumulonimbus (Cb) and nimbostratus (Ns) clouds. In general, what the first approach classifies as nimbostratus (Ns) clouds, the ISCCP approach classifies as altocumulus (Ac) clouds. This is most probably due to the fact that these cloud regions do have precipitation, which is considered an indicator for nimbostratus (Ns) clouds in the first approach but does not have an influence in the second approach. Apart from that, both pictures generally agree with each other and with the preceding insights.

Implementation

We built an interactive visualization tool based on VTK and Qt5. The pathlines are integrated using a fourth-order Runge-Kutta integrator with a step size of 5 s. Since the time steps for the 3-D data is 1 min, the wind fields have to be interpolated for the integration. We compute the pathlines with corresponding vorticity and divergence values on the fly to allow for an interactive exploration of the data. A seeding box can be moved and the pathlines can be colored by vorticity, horizontal divergence, or the updraft. For the coloring, we use color maps from ColorBrewer.[12] Our system is equipped with an Intel Core i7 with 2.3 GHz, 16 GB RAM and an NVIDIA GeForce GT 650M with 512-MB VRAM. The available RAM allows for the computation of pathlines with lengths up to 30 min. The computation and rendering of 1000 pathlines with a length of 20 min take 2.1 s on the highest resolution grid

used with 20 million points. The two FTLE visualizations in Figure 10 were computed on an Nvidia GTX 970 GPU within 7 days (6000 samples per pixel for entire Germany) and 5 days (2000 samples per pixel for Regensburg), respectively.

Conclusion

We visualized the weather situation above Germany on April 26, 2013. We showed CLW, CLI, and QR for the entire domain, which were viewed in the presence of airplane trajectories. For the wind visualizations, we concentrated on orography-induced cloud development and updraft, which we related to divergence and vorticity. We compared different ICON resolutions and to better understand the Lagrangian processes, we employed unbiased FTLE rendering and decoupled opacity optimization. Finally, we extended two 2-D cloud classifications to 3-D.

In the future, we would like to advance the classification methods by improving the spatial smoothness and temporal coherence. Visualizing the differences between historically measured attributes and the reanalysis simulation is an interesting avenue for future work.

References

1. R. Heinze *et al.,* "Large-eddy simulations over Germany using ICON: A comprehensive evaluation," *Quart. J. Roy. Meteorol. Soc.*, vol. 143, no. 702, pp. 69–100, 2017.
2. M. Rautenhaus *et al.,* "Visualization in meteorology - A survey of techniques and tools for data analysis tasks," *IEEE Trans. Vis. Comput. Graph.*, vol. 24, no. 12, pp. 3268–3296, Dec. 2017, doi: 10.1109/TVCG.2017.2779501.
3. Weather station Regensburg/Oberhub. [Online]. Available: http://www.wetteronline.de/rueckblick?gid=10776. Accessed: Jul. 16, 2017.
4. Weather station Bad Lippspringe. [Online]. Available: http://www.wetteronline.de/rueckblick?gid=10430. Accessed: Jul. 16, 2017.
5. M. A. Shapiro, "Turbulent mixing within tropopause folds as a mechanism for the exchange of chemical constituents between the stratosphere and troposphere," *J. Atmos. Sci.*, vol. 37, no. 5, pp. 994–1004, 1980.
6. T. Günther, H. Theisel, and M. Gross, "Decoupled opacity optimization for points, lines and surfaces," *Comput. Graph. Forum (Proc. Eurographics)*, vol. 36, no. 2, pp. 153–162, 2017.
7. T. Günther, A. Kuhn, and H. Theisel, "MCFTLE: Monte carlo rendering of finite-time Lyapunov exponent fields," *Comput. Graph. Forum (Proc. EuroVis)*, vol. 35, no. 3, pp. 381–390, 2016.
8. World Meteorological Organization. International Cloud Atlas, vol. I. WMO, 1975.
9. International satellite cloud climatology project. [Online]. Available: https://isccp. giss.nasa.gov/cloudtypes.html. Accessed: Jul. 16, 2017.
10. G. L. Stephens, "Radiation profiles in extended water clouds. II: Parameterization schemes," *J. Atmos. Sci.*, vol. 35, no. 11, pp. 2123–2132, 1978.
11. S. Erneis, *Wind Energy Meteorology: Atmospheric Physics for Wind Power Generation*. New York, NY, USA: Springer, 2013.
12. M. Harrower and C. A. Brewer, "Colorbrewer.org: An online tool for selecting colour schemes for maps," *Cartographic J.*, vol. 40, no. 1, pp. 27–37, 2003.

Noël Rimensberger is a student with ETH, Zürich, Switzerland. He received the B.Sc. degree in computer science, in 2018, and is currently working toward the M.Sc. degree in computer science with a focus on scientific visualization as well as the design and analysis of algorithms. Contact him at noelr@student.ethz.ch.

Markus Gross is a Professor of computer science with the Swiss Federal Institute of Technology Zürich, Zürich, Switzerland, Head of the Computer Graphics Laboratory, and Director of Disney Research, Zürich, Switzerland. His research interests include physically based modeling, computer animation, immersive displays, and video technology. He received the Ph.D. degree in computer graphics and image analysis from Saarland University, Saarbrücken, Germany, in 1989. Contact him at grossm@inf.ethz.ch.

Tobias Günther joined the Computer Graphics Laboratory, ETH Zürich, Zürich, Switzerland, as a Postdoctoral Researcher, in 2016. His research interests include scientific visualization, progressive light transport, and real-time rendering. He received the M.Sc. degree in computer science and the Ph.D. degree both from the University of Magdeburg, Magdeburg, Germany, in 2013 and 2016, respectively. Contact him at tobias.guenther@inf.ethz.ch.